Widely tunable dual-wavelength operation of Tm:YLF, Tm:LuAG, and Tm:YAG lasers using off-surface optic axis birefringent filters

Article *in* Applied Optics · August 2018

DOI: 10.1364/AO.57.006679

CITATIONS
32

READS
612

2 authors:

Ersen Beyatli
Recep Tayyip Erdoğan Üniversitesi
23 PUBLICATIONS **244** CITATIONS

SEE PROFILE

Umit Demirbas
Antalya Bilim University
180 PUBLICATIONS **1,764** CITATIONS

SEE PROFILE

Widely-tunable dual-wavelength operation of Tm:YLF, Tm:LuAG and Tm:YAG lasers using off-surface optic axis birefringent filters

Ersen Beyatli,[1] Umit Demirbas,[2,*]

[1]*Department of Electrical-Electronics Engineering, Recep Tayyip Erdogan University, Rize, 53100, Turkey*
[2]*Laser Technology Laboratory, Department of Electrical and Electronics Engineering, Antalya Bilim University, 07190 Antalya, Turkey*
**Corresponding author: umit79@alum.mit.edu*

Abstract

In this work, we have demonstrated dual-wavelength continuous-wave laser operation in diode-end-pumped Tm:YLF, Tm:LuAG and Tm:YAG lasers. A 3-mm thick quartz birefringent filter with an optical axis 45° to the surface plane was exploited for achieving broadly-tunable two-color laser operation. By using the different orders of the filter with varying filter width and free spectral range values, dual-wavelength operation has been achieved in 11, 12 and 8 different wavelength pairs in Tm:YLF, Tm:LuAG and Tm:YAG, respectively. Fine tuning of the rotation angle of the birefringent filter enabled control of laser power in each line. To our knowledge, this is the first report of multicolor laser operation in these gain media, and the technique used is applicable to other laser operation regimes including mode-locking.

1. Introduction

Dual-wavelength (two-color, multicolor) solid-state laser operation is the simultaneous oscillation of more than one laser wavelength in the laser resonator. This operation regime might be advantageous for applications such as coherent terahertz (THz) wave generation [1-3], ultrahigh pulse repetition rate creation by optical beating [4], laser ranging [5], remote sensing [6], digital holographic microscopy [7], optical communication [8, 9], and coherent anti-Stokes Raman scattering microscopy [10]. In recent years, usage of intracavity birefringent filters (BRFs) was proposed as a flexible method for the generation of multicolor laser operation. In regular BRFs, which are also known as on-surface optic axis BRFs, the optic axis lies on the surface of the plate. Using regular BRFs, dual-wavelength radiation has been successfully demonstrated in Ti:Sapphire [11, 12], Yb:KGW [13], Yb:CALGO [14], Nd:YVO4 [15], and Alexandrite [16].

In most studies regular BRFs are implemented due to easiness in fabrication; however, this specific case is not necessarily an optimum choice [17-21]. As an alternative to regular BRFs, birefringent filters with optic axis pointing out of its surface could provide a much broader set of filter parameters [17-21]. Off-surface optic axis BRFs could scan larger number of filter orders providing flexibility in choosing the optimum filter bandwidth (FWHM) and free spectral range (FSR) value for the desired application [19]. Moreover, they could provide a smoother variation of modulation depth as the wavelength is tuned [19]. Off-surface optic axis BRFs have already been used in demonstrating multicolor laser operation in more than 10 pairs of transitions in Cr:LiSAF [22] and Cr:Nd:GSGG [22, 23].

In Thulium-doped laser gain media, two-color laser operation has been demonstrated in Tm:CYA (1959 & 1961 nm [24]), Tm:YAP (1940 & 1986 nm [25], 1969 & 1979 nm [26]), Tm:Lu_2O_3 (1968 & 2068 nm [27]), Tm:Ho:YAG (2090 & 2096 nm [28]), Tm:Ho:$GdVO_4$ (2039 & 2050 nm [29]), Tm:Ho:YVO_4 (2041 & 2055 nm [30]) and Tm:Ho:GYTO (1950 & 2070 nm, 1950 & 2068 nm [31]). Dual-wavelength operation has been shown in continuous-wave (cw) [28-31], gain-switched [27], Q-switched [25, 26, 31] and cw mode-locked [24] operation regimes. Multicolor operation has been achieved via usage of laser crystals with two strong and equal magnitude emission peaks [29], or by employing disordered crystals with multiple emission centers with different emission wavelengths [24], or via interesting coupling of spectral and temporal dynamics [27]. In most of these studies, two-color lasing has been achieved in just one pair of wavelengths, and mechanism that is used for multicolor operation did not allow flexible control of two-color laser parameters.

In this study, using a 3-mm thick, off-surface optic axis crystalline quartz BRF with an optic axis 45° to the surface of the plate, we have achieved stable broadly-tunable dual-

wavelength cw laser operation in diode-end-pumped Tm:YLF, Tm:LuAG and Tm:YAG lasers. Optimization of the rotation angle of the intracavity inserted BRF filter around different orders (rotation angles) facilitated two-color laser operation in 11, 12 and 8 different wavelength pairs in Tm:YLF, Tm:LuAG and Tm:YAG, respectively. For most of the cases, fine tuning of the rotation angle enabled adjustment of laser power in each line. The wavelength separation between the lines could be varied between 14 and 192 nanometres. To our knowledge, this is the first report of multicolor laser operation in Tm:YLF, Tm:LuAG and Tm:YAG gain media. Moreover, the demonstrated wide-tunability of two-color laser wavelengths is also quite rare in literature.

In terms of the method employed, this study further proves the advantages of off-surface optic axis BRFs in multicolor laser wavelength generation such as lower cost, simpler operation, and flexibility in usage: (i) one device enabling multicolor laser operation in many different wavelength pairs, (ii) ability to control laser power in each line, (iii) capability to use a rich number of filter parameters from a single BRF plate, (iv) effectiveness in cw, gain-switched, Q-switched and cw mode-locked regimes, and (v) universal usage of the device in any laser that lies within the transmission bandwidth of the BRF plate (250-2500 nm quartz BRFs [19, 22, 23]).

2. Experimental setup

Figure 1 shows a schematic of the diode pumped Tm:YLF, Tm:LuAG and Tm:YAG laser cavities used in cw dual-wavelength laser experiments. A linearly polarized 3-W single-emitter multimode laser diode (MMD) operating at 780 nm was used as the pump source. The pump beam was first collected with an aspheric lens with focal length of f=4.5 mm (f1). Then, a cylindrical lens with a focal length 5-cm (fz) was employed for fast axis collimation, and a plano-convex lens with a 5-cm focal length was utilized for focusing the pump beam into the crystal. Variation of the diode current changes the output wavelength and output beam profile. Therefore, the diode current is kept at 3 A in all the experiments. A polarizing beam splitter cube (PBS) and a half-wave plate (HWP) were used to adjust the incident pump power on the crystals. The maximum incident pump power on the crystals was 2.45 W (lower than 3 W due to the transmission losses of the optics).

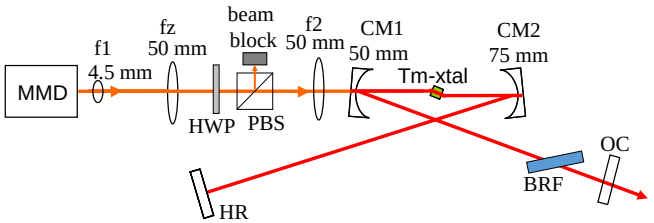

Fig. 1 Schematic of the multimode diode pumped cw Tm:YLF, Tm:LuAG and Tm:YAG lasers used in dual-wavelength laser studies. HWP: Half-wave plate, MMD: multimode diode, PBS: polarizing beam splitter cube, BRF: birefringent filter, HR: flat high reflector, CM1-CM2: Curved cavity high reflectors, OC: output coupler.

The cw laser experiments were based on an astigmatically-compensated X-cavity consisting of two curved mirrors (CM1 ROC =50 mm and CM2 ROC = 75 mm), a flat end mirror (HR) and a 1.3% transmitting flat output coupler (OC). The length of the long cavity arm has been adjusted to 30 cm to obtain a beam waist of approximately 40 μm inside the gain medium. The HR mirrors had a reflectivity greater than 99.9% from 1850 nm to 2200 nm and a pumping window with transmission around 95% in the red spectral region. Brewster-cut, 5-mm-long, Tm:YLF, Tm:LuAG and Tm:YAG crystals with Tm^{+3}-concentration of 3%, 6% and 6% were used in the study. The crystals absorbed 73%, 82% and 85% of the incident TM polarized pump light at 780 nm, respectively. To optimize laser properties, the crystals were cut so that, for TM polarized incident light, the direction of the electric field of the electromagnetic wave inside the crystal is parallel to the crystal c (π) axis. As mentioned earlier, a 3-mm-thick crystal quartz BRF with an optic axis 45° to the surface of the plate was used as the wavelength selective element in tunable single wavelength and dual-wavelength laser experiments.

3. Free-running cw lasing results and tunable single-wavelength operation

In this section we will briefly present cw lasing results obtained with the aforementioned Tm-doped crystals in free running and in tunable single-wavelength operation. Figure 2 shows the measured cw efficiency curves of the Tm:YLF, Tm:LuAG and Tm:YAG lasers using a 1.3% transmitting output coupler. Continuous-wave laser output powers as high as 535 mW, 585 mW and 550 mW were obtained at the full incident pump power level of 2450 mW from the Tm:YLF, Tm:LuAG and Tm:YAG lasers, respectively. The corresponding slope efficiency with respect to incident laser power were 25%, 26% and 28%, and the free running laser wavelengths were 1940 nm, 2025 nm and 2015 nm.

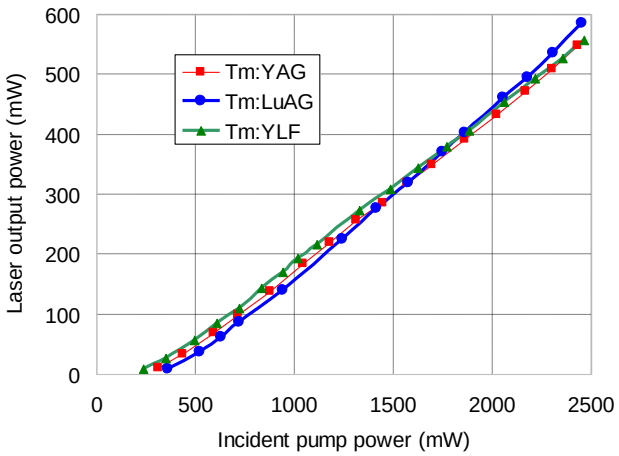

Fig. 2 Measured cw output power of the multimode diode pumped Tm:YLF, Tm:LuAG and Tm:YAG lasers as a function of incident pump power at an output coupling of 1.3%.

We have investigated the single-wavelength tuning behavior of the lasers using the BRF plate as the tuning element. Fig. 3 shows the variation of the measured output power from the Tm:YLF, Tm:LuAG and Tm:YAG lasers as a function of wavelength using the 1.3% transmitting output coupler (a normalized scale is used on purpose for comparison purposes). Fig. 3 also displays the measured transmission profile of the output coupler (OC), as well as the high reflector (HR) mirrors used in the cavity. The calculated total leakage loss from the cavity optics (5 bounces on HR, and 1 bounce on OC) is also shown. Note that as mentioned earlier, the cavity high reflectors start to leak at wavelengths below 1900 nm, creating substantial loss especially below 1850 nm.

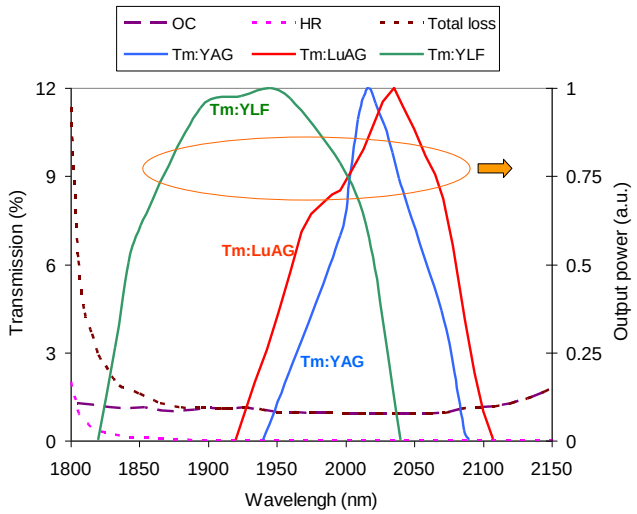

Fig. 3 Measured single-wavelength tuning range of Tm:YLF, Tm:LuAG and Tm:YAG at the full incident pump power of 2.45 W using a 1.3% transmitting output coupler. Measured transmission of the output coupler (OC) and cavity high reflective mirrors, and calculated total leakage loss of the cavity (OC+5HR) are also shown.

In our laser cavity, among the Tm-based gain media studied in this work, Tm:YLF provided the broadest, smoothest and most symmetric single-wavelength tuning spectrum, with a full-width at half-maximum (FWHM) of 200 nm centered around 1940 nm. Tm:LuAG and Tm:YAG have tuning bandwidths of 130 nm and 75 nm centered around 2025 nm and 2015 nm, respectively. We would like to clearly emphasize here that, these numbers are specific to our setup, and could be different for other systems due to difference in reflectivity properties of cavity optics used as well as due to the quasi-3-level laser structure of the Tm^{+3}-ion at this wavelength region, which creates inversion (pump power) dependent gain/tuning spectrum. As an example, in the case of Tm:YLF the limited reflectivity of the cavity high reflectors substantially limited the obtainable tuning range and output powers below 1850 nm [32]. Moreover, in our setup, the cavity high reflectors reflectivity extend up to 2200 nm in the long wavelength side, which prevents tuning of Tm:YLF around 2300 nm [33].

4. Theoretical background and numerical analysis for dual-wavelength operation

Dual-wavelength laser operation requires balancing of laser gain simultaneously at two different wavelengths within the gain bandwidth of the laser active medium. To be more specific, as pointed by Waritanant et al., the BRF could be used to fine tune the intracavity losses so that, the oscillating wavelengths has similar lasing thresholds, slope efficiencies and output powers [15]. Usually the BRF angle is tuned to achieve same output power levels at λ_1 and λ_2 at a given pump power P_{pump}:

$$P_{out,\lambda 1}(P_{pump}) = P_{out,\lambda 2}(P_{pump}) \quad (1)$$

which can be rewritten as:

$$\eta_{\lambda 1}(P_{pump}-P_{th,\lambda 1}) = \eta_{\lambda 2}(P_{pump}-P_{th,\lambda 2}) \quad (2)$$

where $P_{th,\lambda 1}$ ($P_{th,\lambda 2}$) is the lasing threshold pump power for wavelength λ_1 (λ_2), and $\eta_{\lambda 1}$ ($\eta_{\lambda 2}$) is the laser slope efficiency at the wavelength λ_1 (λ_2).

To elaborate this issue further, we can look back again to Fig. 3, which provides information on the variation of single-line laser performance with wavelength for our specific cavity at hand. As an example assume that we want to get dual-wavelength lasing at 1850 nm and 2000 nm in Tm:YLF. To achieve this, first of all one needs to suppress the gain peak of Tm:YLF at around 1940 nm. Moreover, the gain at 1850 and 2000 nm should be roughly equalized. This could be achieved by use of an intracavity BRF with a free spectral range (FSR) around 150 nm, where the transmission peaks of the filter are centered around 1850 and 2000 nm. Exact positions of the transmission peaks could be adjusted by fine tuning of the BRF filter rotation angle. In this scheme, by using different FSR values of the BRF plate located at different orders, one can obtain dual-wavelength operation with different wavelength separation values (λ_2-λ_1). The scheme described above is one of the methods that could be used for achieving dual-wavelength operation using BRFs (method 1: both lasing lines centered at transmission maxima of the BRF).

As another method (method 2), assume we want to generate dual-wavelength operation in Tm:YAG at 2000 & 2015 nm (one wavelength around the gain peak, and another one slightly to the left). Note that for this case the desired wavelength separation is quite small, which makes implementation of method 1 rather difficult for reasonably thick BRFs. As an alternative, to achieve two-color laser operation for this case, one can use a BRF filter with a transmission peak around 2000 nm (centered at the weaker line). If the filter has a suitably large transmission passband bandwidth (FWHM), the

filter could suppress the gain at 2015 nm just enough to balance gain at both wavelengths. As a result simultaneous two-color laser operation could be achieved. In this 2nd method, by using different FWHM values of the BRF plate located at different orders, one can obtain dual-wavelength operation with different wavelength separation values (λ_2-λ_1). Note that filter FWHM could also be altered by using additional polarizing elements in the cavity [18, 19]. In our experiments, we have seen dual-wavelength operation based on both of these methods (later see Fig. 10 and Fig. 11 as representative examples). For both methods, it is clear that, a BRF filter with a rich set of FSR and FWHM values has advantages in achieving multicolor laser operation.

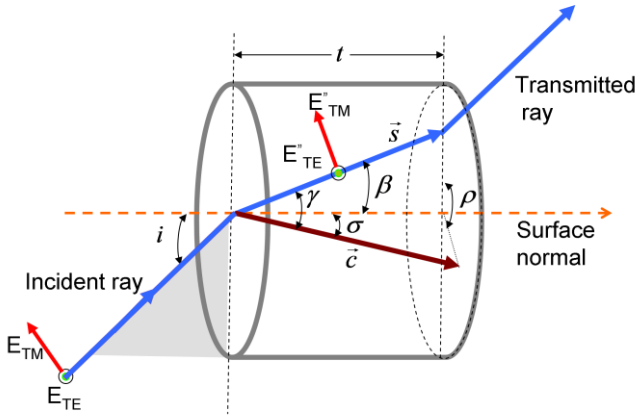

Fig. 4 Light beam incident on an off-surface optic axis birefringent filter plate at Brewster's angle [19, 21]. t: thickness of the plate, $\vec{c}$: optic axis of the plate, ρ: rotation angle of the plate, $\vec{s}$: direction of beam propagation, σ: angle between the optic axis and the surface normal, i: incidence angle (55.2° in quartz at 2 μm), β: internal Brewster's angle.

In that respect, at this point, we would like to briefly discuss the advantages of off-surface optic axis BRFs compared to regular on-surface optic axis ones [17-19]. For this purpose, Fig. 4 shows the laser light path in a typical BRF inserted in standing-wave laser cavity at Brewster's angle (detailed definitions of relevant physical parameters are given in the figure). For the regular on-surface optic axis BRF, the optic axis lies on the surface of the plate and σ = 90°. Tuning of the laser wavelength and adjustment of dual-wavelength operation is facilitated simply by rotation of the birefringent plate about an axis normal to the surface (corresponds to changing ρ, in Fig. 4). One needs to find the polarization eigenmodes and eigenvalues of the overall Jones matrix of the laser cavity to calculate the round-trip transmission characteristic of the BRF containing resonator [17-21].

Following the work in [17-21], one can show that the free spectral range of the filter can be calculated using:

$$FSR = \frac{\lambda^2 Cos(\beta)}{t\Delta n Sin^2(\gamma)} . \quad (3)$$

Equation (3) could also be re-written as:

$$FSR = \frac{\lambda}{m} , \quad (4)$$

where m is the filter order number. For example, for a specific wavelength of λ, when m=1, the phase retardation (Δφ) created by the birefringent plate is 2π (meaning no change in input polarization state), and the filter has a transmission maxima at this λ at the filter order of m=1, with a filter FSR of λ. In general, when Δφ=m2π holds, the filter will have a transmission maxima at λ, at the filter order of m, and with an FSR value of λ/m. Hence, the FSR values that could be achieved from the system is quantized and one could only attain discrete FSR values of λ/m. Moreover, not all m values are allowed (or achievable), and permissible set of m values depend on filters thickness and optic axis diving angle σ. A similar relation can also be shown for the filters FWHM value, where the achievable FWHM scales with 1/m (filter FWHM also depends on the polarization dependent losses in the cavity). Hence, a BRF filter with a broader set of filter orders (m values) is desired, since a broader set of m values results in a broader set of achievable FSR and FWHM values.

To deepen the discussion on this issue further, Fig. 5 shows the calculated variation of filter FSR with filter rotation angle ρ. The calculation has been performed at a central wavelength of 2 μm, for several different optic axis orientations (σ) in the range from 0° and 90° (t=3mm). The x-axis has been limited to plate rotation angle values from ρ=0° to ρ=180°, since the 180°-360° range is a symmetric copy. The solid lines have been calculated using Eq. (3), and the dots on the solid lines are the resonance points satisfying Eq. (4). Similarly, the dashed gray horizontal lines in the figure indicates the λ/m values, at selected m values of 1, 2, 3, 5, 10 and 20.

As an important observation, we see clearly from Fig. 5 that, birefringent filters diving angle (σ) significantly effects the range of FSR values that can be obtained. In other words, BRFs diving angle (σ) determines which m values are allowed for a given filter thickness at a specific central wavelength [19]. Especially note that, for on-surface optic axis BRF (σ=90°), the obtainable FSR values are quite small and varies in a very narrow range (140-180 nm). This is because a 3 mm thick quartz on-surface optic axis BRF enables accessing plate orders (m) between 11 and 14 only, and this limits the obtainable FSR values to roughly between λ/11≈181 nm and λ/14≈143 nm. Note that for the BRF we have at hand (σ=45°, t=3mm), filter orders from m=1 to

m=14 is accessible, resulting in FSR values between 143 and 2000 nm.

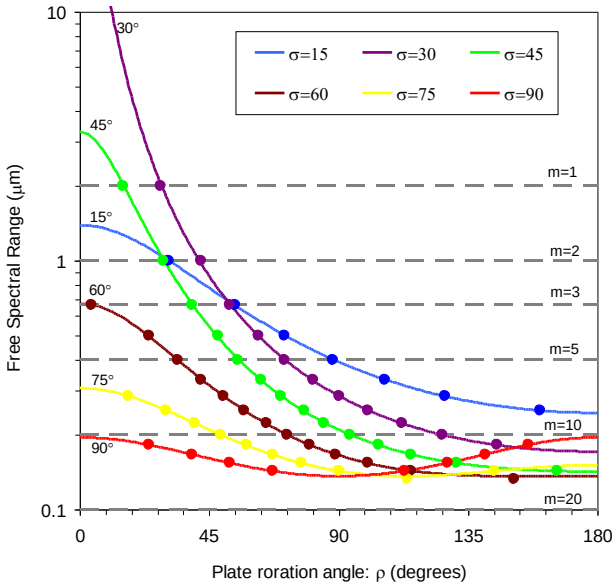

Fig. 5 Calculated variation of free spectral range for a standing-wave Tm-based laser cavity around 2 μm, as a function of birefringent plate rotation angle (ρ). The calculation has been performed for different optic axis orientation values σ ranging between 0° and 90°. The quartz birefringent plate was assumed to have a thickness of 3 mm.

Fig. 6 shows the calculated round-trip transmission properties of our cavity (Fig. 1), with the Tm:YLF laser crystal. Both the BRF and the gain medium were assumed to be inserted at Brewster's angle. The transmission is calculated for all the supported filter orders (m) between 1 and 14. The corresponding resonant rotation angle (ρ) values that provide a transmission maxima at 2000 nm are: 15.3° (m=1), 29.3° (m=2), 39.2° (m=3), 47.6° (m=4), 55.3° (m=5), 62.7° (m=6), 70.1° (m=7), 77.6° (m=8), 85.5° (m=9), 93.9° (m=10), 103.5° (m=11), 115.1° (m=12), 130.7° (m=13), 165.8° (m=14). Figure 6 is prepared for Tm:YLF, but the general properties of the filter will be similar in Tm:LuAG and Tm:YAG as well (transmission peak positions will not change, but the modulation depth values will differ due to difference in refractive index values: same filter FSR, slightly different filter FWHM [19]).

Note from Fig. 6 that as the plate's rotation angle (or order of the filter) is varied, the filter properties such as modulation depth, FSR and FWHM of the transmission peaks change considerably. The achievable filter FSR values roughly cover the 150-2000 nm range, where as the filter FWHM values vary between 10 and 150 nm. This large set of available filter parameters, is due to the off-surface optic axis BRF used in this study, which enables dual-wavelength laser operation in record number of wavelength pairs as we will discuss below. We refer the reader to [19] for a detailed discussion on the effect of filter orders on tuning rate, modulation depth, and walk-off angle.

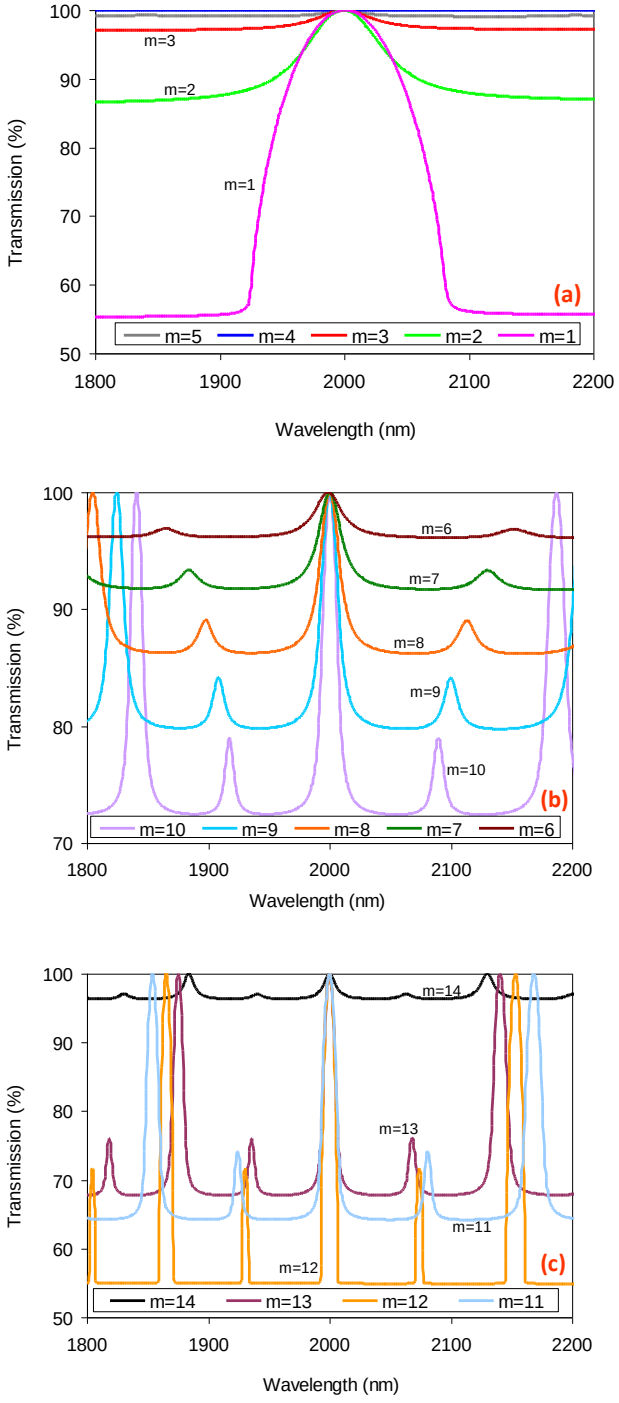

Fig. 6 Calculated transmission characteristics of the Tm:YLF laser cavity as a function of wavelength around the central wavelength of 2 μm for different birefringent plate orders (m) between 1 and 14. The calculation has been performed for a 3-mm-thick crystal quartz BRF with an optic axis tilted 45° with respect to the surface of the plate.

5. Tunable dual-wavelength lasing results

Figure 7, 8 and 9 show the tunable cw dual-wavelength operation results obtained with Tm:YLF, Tm:LuAG and Tm:YAG lasers respectively. Measured power levels from the lasers at each dual-wavelength pair are also indicated in the figure (at the maximum available incident pump power of 2.45 W).

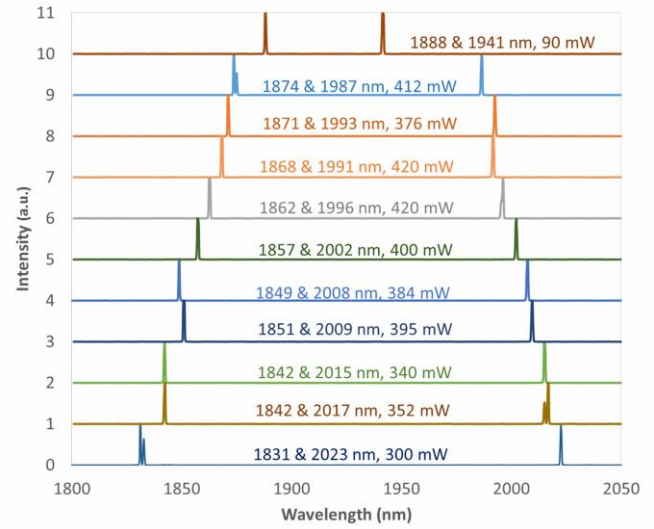

Fig. 7 Optical spectra obtained in dual-wavelength operation of the cw Tm:YLF laser at an incident pump power of 2.45 W. Achieved output powers are also indicated for each case.

The Tm:YLF laser could be operated in dual-wavelength operation quite stably at 11 different laser wavelength pairs (Fig. 7): 1831 & 2023 nm, 1842 & 2017 nm, 1842 & 2015 nm, 1851 & 2009 nm, 1849 & 2008 nm, 1857 & 2002 nm, 1862 & 1996 nm, 1868 & 1991 nm, 1871 & 1993 nm, 1874 & 1987 nm and 1888 & 1941 nm, respectively. For most of the cases by fine adjusting the BRF plate rotation angle, it was possible to equalize laser power in each line. Also, what is shown in Fig. 7 is only sample spectra, and it was possible to fine tune the dual-wavelength spectra 1-2 nanometers to the left or to the right by fine adjustment of the BRF rotation angle. Moreover, there were many other wavelength pairs (not reported here), where the two-color laser operation has been observed with fluctuating output. The reported lines in Fig. 7 provided long term stable laser output with minimal power fluctuations. Note that our laser system was not covered, and we believe that with an engineered laser system with control electronics could enable multicolor lasing in a much broader set of wavelengths. Note that the central wavelength ($(\lambda_1+\lambda_2)/2$) of the reported lasing lines in Fig. 7 is around 1930 nm, which is very close to the free running lasing wavelength in Tm:YLF (1940 nm). The wavelength separation between the lines could be varied between 53 nm and 192 nm, by use of different rotation angles of the BRF filter. The output powers in dual-wavelength operation was above 350 mW for most cases. The line widths of the optical spectrum could not be measured due to the limited resolution of the spectrometer used, but was confirmed to be below 0.5 nm in all cases. As an interesting point, note from earlier analysis that the FWHM of the BRF filter is calculated to vary in the 10-150 nm range. However, these values correspond to single round-trip filtering effect. During cw laser operation, the laser observes the BRF filter many times, and the effective filter bandwidth is much narrower (10s to 100s of picometers, depending also on the cavity photon lifetime) [21].

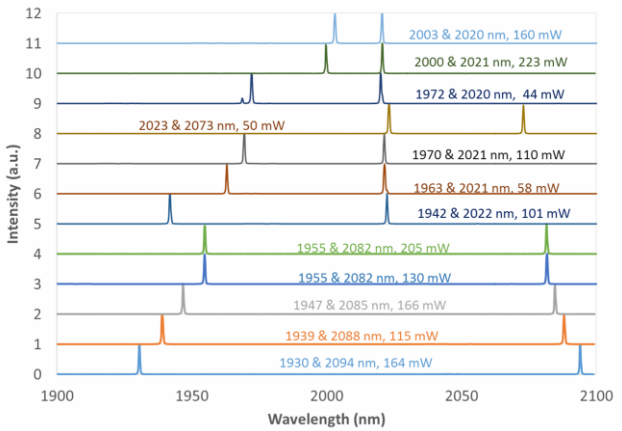

Fig. 8 Optical spectra obtained in dual-wavelength operation of the cw Tm:LuAG laser.

In the case of Tm:LuAG, stable two-color laser operation has been achieved at 12 different laser wavelength pairs (Fig. 8): 1930 & 2094 nm, 1939 & 2088 nm, 1947 & 2085 nm, 1955 & 2082 nm, 1956 & 2082 nm, 1942 & 2022 nm, 1963 & 2021 nm, 1970 & 2021 nm, 2023 & 2073 nm, 1972 & 2020 nm, 2000 & 2021 nm, and 2003 & 2020 nm, respectively. The average central wavelength of the lasing lines is around 2010 nm, which is relatively close to the free running lasing wavelength in Tm:LuAG (2025 nm). The wavelength separation between the lines varied between 17 nm and 164 nm. The output powers in dual-wavelength operation was relatively low (compared to free running cw operation), and was mostly between 100-200 mW level. We believe the observed difference in the distribution of dual-wavelength laser line pairs and the difference in output powers between Tm:YLF and Tm:LuAG is due to the broader and smoother tuning curve of Tm:YLF (Fig. 3), which enabled higher efficiencies in two-color operation. Basically, the relatively thin (3 mm) BRF plate that was used in this study was a better match for gain media with a tuning range (FWHM) broader than 100 nm.

Finally, with Tm:YAG gain medium, stable two-color operation has been realized at 8 different laser wavelength pairs (Fig. 9): 1945 & 2082 nm, 1953 & 2080 nm, 2015 & 2077 nm, 1953 & 2014 nm, 1961 & 2011 nm, 1965 & 2010 nm, and 1993 & 2007 nm, respectively. Similar to Tm:LuAG, the average central wavelength of the lasing lines is around 2010 nm, which is very close to the free running lasing wavelength in Tm:YAG (2015 nm). The wavelength

separation between the lines varied between 14 nm and 137 nm. The average output power in dual-wavelength operation was around 100 mW. Note that, dual-wavelength operation results of Tm:YAG is similar to Tm:LuAG due to similarities in gain spectrum, Tm:LuAG providing slightly better results (higher output powers) probably because of its slightly broader tuning profile. We also note here that, the BRF sample we have used in this work (3 mm thick crystal quartz with an optical axis 45° to the surface plane) was chosen due to its availability from an earlier study, and it is not necessarily an optimum choice. We foresee that obtained dual-wavelength operation could be improved by using an off-axis BRF with an optimized thickness and optic axis diving angle [19]. For example, usage of a thicker BRF could enable accessing smaller FSR values, which could enable efficient two-color operation in Tm:YAG and Tm:LuAG lasers as well. More specifically, we recommend usage of 5-10 mm thick quartz a birefringent filters with an optic axis diving angle (σ) of 25° in future multicolor lasing studies with Tm-doped gain media [19].

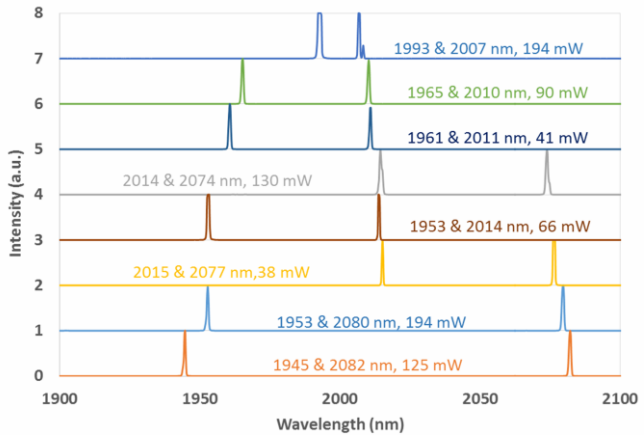

Fig. 9 Optical spectra obtained in dual-wavelength operation of the cw Tm:YAG laser.

In closing this section, we would like to discuss whether the tuning results obtained with the off-surface optic axis BRF can be explained with the numerical analysis described in Section 4. Before we start, we note here that, in general the physics of Eq. (2), generating simultaneous dual-wavelength laser operation with same/similar output power in each line is rather involved. The physics underlying Eq. (2) requires careful usage of generally wavelength dependent laser parameters such as effective stimulated emission cross section, excited state absorption cross section, Auger upconversion rate, Stark component distribution, self absorption loss, passive cavity loss, cavity spot size, etc… [27, 32, 34]. Hence, in reality each of these factors should be taken into account to fully analyze the situation and calculate the required differential modulation depth from the BRF for the generation of equal power dual-wavelength operation. On the other hand, as we will demonstrate with two representative examples below, the simplified picture we have presented above makes a good enough job in roughly understanding the basics of dual-wavelength operation with BRFs.

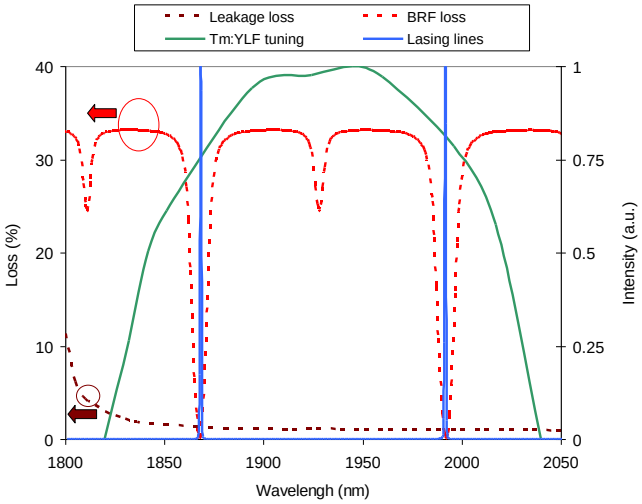

Fig. 10 Detailed analysis of synchronous dual-wavelength cw laser operation in Tm:YLF at 1868 & 1991 nm pair (420 mW output power). Dual-wavelength operation has been achieved at a BRF plate rotation angle (ρ) of around 130°. The calculated cavity round-trip travel losses induced by the BRF as well as the estimated total cavity leakage loss are also shown.

As the first example lets consider dual-wavelength operation of Yb:YLF at laser wavelengths of 1868 and 1991 nm (Fig. 10). This pair of wavelengths produced an output power of 420 mW, which is very close to what can be achieved in free running operation (535 mW). Dual-wavelength operation has been achieved at a BRF rotation angle (ρ) of around 130°. Figure 10 shows the calculated losses induced by the BRF plate (100% - BRF Transmission), as well as the Yb:YLF tuning curve and optical spectrum of the two-color laser. Note that, the lasing lines are located at the maxima of BRF plate transmission (or minima of BRF induced cavity losses). Moreover, since the BRF introduces no additional intentional losses at the lasing wavelengths, the achieved output power level in two-color laser operation is also quite high. This example demonstrates the usage of method 1 in achieving multicolor laser operation (see Section 4).

As another representative example, Fig. 11 shows dual-wavelength operation data for Yb:LuAG at laser wavelengths of 2000 & 2021 nm. For this case, dual-wavelength operation has been achieved at a BRF rotation angle (ρ) of around 15°. At this rotation angle, filter order is 1 (m=1), and we have a very broad filter FWHM. The BRF filter transmission maxima (or filter loss minima) is located around 2000 nm. One of the lasing lines (the weak line) is located at this transmission maxima, and the second laser line is located at 2021 nm, where the laser emission is stronger. At 2021 nm, the additional BRF loss balances the higher gain and enables synchronous dual-wavelength operation with the weaker 2000 nm line (method 2). The output power in two-color operation is relatively low

(223 mW), partly due to the additional loss introduced by the BRF to balance gain.

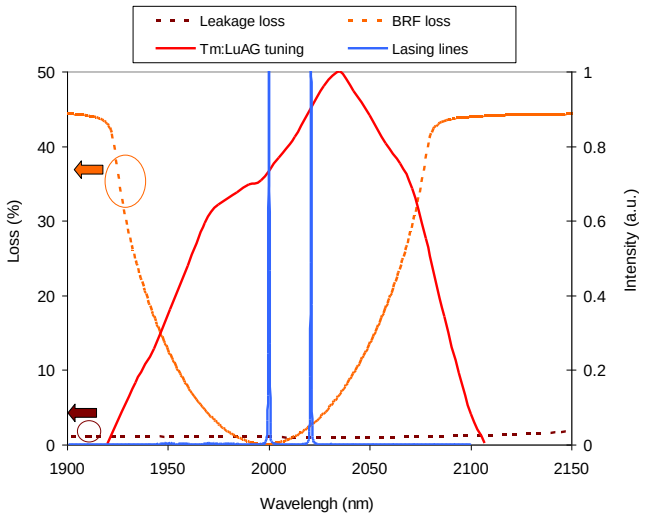

Fig. 11 Detailed analysis of synchronous dual-wavelength cw laser operation in Tm:LuAG at 2000 & 2021 nm pair (223 mW output power). Dual-wavelength operation has been achieved at a BRF plate rotation angle (ρ) of around 15°. The calculated cavity round-trip travel losses induced by the BRF as well as the estimated total cavity leakage loss are also shown.

In summary, we have seen from these two representative examples that, our simple analysis could be used to roughly understand and predict multicolor laser operation in Tm-doped lasers. On the other hand, a mathematically more rigorous analysis involving detailed laser physics is recommended for a deeper understanding of the phenomena. Our simple analysis and experimental results just show the potential of off-surface optic axis BRFs in achieving superior performance in multicolor laser operation compared to other widely used methods.

6. Conclusion

In conclusion, we have acquired broadly-tunable dual-wavelength laser operation in three different Tm^{3+} doped laser systems using a 3-mm-thick crystal quartz BRF with an optic axis 45° to the surface of the plate. Two-color laser operation has been demonstrated in 11, 12 and 8 different wavelength pairs in Tm:YLF, Tm:LuAG and Tm:YAG, respectively. Simulation results has been used to explain/predict the observed results. To our knowledge, this is the first report of dual-wavelength operation in these gain media. The BRF sample used in this study was also used in earlier cw and femtosecond tuning experiments with Cr:LiSAF [35], for dual-wavelength laser operation in Cr:LiSAF [22] and Cr:Nd:GSGG [22, 23], showing the universality and extensive usage potential of off-surface optic axis BRFs for many applications. In this study, only cw results are presented, but it is possible to use this method in mode-locked regime to obtain dual-wavelength cw mode-locked operation with picosecond level pulses, as it was already demonstrated in Cr:Nd:GSGG[23]. We foresee that usage of thicker BRFs (5-10 mm) could enable even better multicolor laser performance in future studies with Tm-based lasers.

Acknowledgements

This work was supported in part by the Scientific and Technological Research Council of Turkey (TUBİTAK) under grant 115F053.

References

1. K. Kawase, M. Mizuno, S. Sohma, H. Takahashi, T. Taniuchi, Y. Urata, S. Wada, H. Tashiro, and H. Ito, "Difference-frequency terahertz-wave generation from 4-dimethylamino-N-methyl-4-stilbazolium-tosylate by use of an electronically tuned Ti:sapphire laser," Optics Letters **24**, 1065-1067 (1999).
2. P. Gu, F. Chang, M. Tani, K. Sakai, and C.-L. Pan, "Generation of Coherent cw-Terahertz Radiation Using a Tunable Dual-Wavelength External Cavity Laser Diode," Japanese Journal of Applied Physics **38**, L1246-L1248 (1999).
3. M. Scheller, J. M. Yarborough, J. V. Moloney, M. Fallahi, M. Koch, and S. W. Koch, "Room temperature continuous wave milliwatt terahertz source," Optics Express **18**, 27112-27117 (2010).
4. M. D. Pelusi, H. F. Liu, D. Novak, and Y. Ogawa, "THz optical beat frequency generation from a single mode locked semiconductor laser," Applied Physics Letters **71**, 449-451 (1997).
5. J. B. Abshire, "Pulsed multiwavelength laser ranging system for measuring atmospheric delay," Applied Optics **20**, 3436-3440 (1980).
6. R. Gaultona, F. M. Dansonb, F. A. Ramirezb, and O. Gunawanb, "The potential of dual-wavelength laser scanning for estimating vegetation moisture content," Remote Sensing of Environment **132**, 32-39 (2013).
7. J. Kühn, T. Colomb, F. Montfort, F. Charrière, Y. Emery, E. Cuche, P. Marquet, and C. Depeursinge, "Real-time dual-wavelength digital holographic microscopy with a single hologram acquisition," Optics Express **15**, 7231-7242 (2007).
8. S. Pan, X. Zhao, and C. Lou, "Switchable single-longitudinal-mode dual-wavelength erbium-doped fiber ring laser incorporating a semiconductor optical amplifier," Optics Letters **33**, 764-766 (2008).
9. C. W. Chow, C. S. Wong, and H. K. Tsang, "All-optical NRZ to RZ format and wavelength converter by dual-wavelength injection locking," Optics Communications **209**, 329–334 (2002).
10. F. Ganikhanov, S. Carrasco, X. S. Xie, M. Katz, W. Seitz, and D. Kopf, "Broadly tunable dual-wavelength light source for coherent anti-Stokes Raman scattering microscopy," Optics Letters **31**, 1292-1294 (2006).
11. C. G. Treviño-Palacios, C. Wetzel, and O. J. Zapata-Nava, "Design of a Dual Wavelength Birefringent Filter " in *RIAO/OPTILAS 2007* N. Wetter, and J. Frejlich, eds. (AIP Conference Proceedings Campinas, São Paulo (Brazil), 2007), pp. 392-397.
12. C. G. Trevino-Palacios, O. J. Zapata-Nava, E. V. Mejia-Uriarte, N. Qureshi, G. Paz-Martinez, and O. Kolokolstev, "Dual wavelength continuous wave laser using a birefringent filter," Journal of the European Optical Society - Rapid publications **8**, 13021 (2013).
13. R. Akbari, H. Zhao, and A. Major, "High-power continuous-wave dual-wavelength operation of a diode-pumped Yb:KGW laser," Opt. Lett. **41**, 1601-1104 (2016).
14. S. Manjooran, P. Loiko, and A. Major, "A discretely tunable dual-wavelength multi-watt Yb:CALGO laser," Appl. Phys. B **124** (2018).
15. T. Waritanant, and A. Major, "Dual-wavelength operation of a diode-pumped Nd:YVO4 laser at the 1064.1 & 1073.1 nm and 1064.1 & 1085.3 nm wavelength pairs," Appl. Phys. B **124** (2018).
16. S. Ghanbari, and A. Major, "High power continuous-wave dual-wavelength alexandrite laser," Laser Physics Letters **14** (2017).
17. K. Naganuma, G. Lenz, and E. P. Ippen, "Variable Bandwidth Birefringent Filter for Tunable Femtosecond Lasers," IEEE J. Quantum Electron. **28**, 2142-2150 (1992).
18. S. M. Kobtsev, and N. A. Sventsitskay, "Application of birefringent filters in continuous-wave tunable lasers: a review," Opt. Spectrosc. **73**, 114-123 (1992).

19. U. Demirbas, "Off-surface optic axis birefringent filters for smooth tuning of broadband lasers," Appl. Opt. **56**, 7815-7825 (2017).
20. S. Zhu, "Birefringent filter with tilted optic axis for tuning dye lasers: theory and design," Appl. Opt. **29**, 410-415 (1990).
21. S. Lovold, P. F. Moulton, D. K. Killinger, and N. Menwk, "Frequency Tuning Characteristics of a Q-Switched Co:MgF_2 Laser " IEEE J. Quantum Electron. **QE-21**, 202-208 (1985).
22. U. Demirbas, R. Uecker, J. G. Fujimoto, and A. Leitenstorfer, "Multicolor lasers using birefringent filters: experimental demonstration with Cr:Nd:GSGG and Cr:LiSAF," Opt. Express **25**, 2594-2607 (2017).
23. T. Yerebakan, U. Demirbas, S. Eggert, R. Bertram, P. Reiche, and A. Leitenstorfer, "Red diode pumped Cr:Nd:GSGG laser: two-color mode-locked operation," J. Opt. Soc. Am. B **34**, 1023-1032 (2017).
24. L. C. Kong, Z. P. Qin, G. Q. Xie, X. D. Xu, J. Xu, P. Yuan, and L. J. Qian, "Dual-wavelength synchronous operation of a mode-locked 2-mu m Tm:CaYAlO4 laser," Opt. Lett. **40**, 356-358 (2015).
25. B. Q. Yao, Y. Tian, G. Li, and Y. Z. Wang, "InGaAs/GaAs saturable absorber for diode-pumped passively Q-switched dual-wavelength Tm:YAP lasers," Opt. Express **18**, 13574-13579 (2010).
26. H. K. Zhang, J. L. He, Z. W. Wang, J. Hou, B. T. Zhang, R. W. Zhao, K. Z. Han, K. J. Yang, H. K. Nie, and X. L. Sun, "Dual-wavelength, passively Q-switched Tm:YAP laser with black phosphorus saturable absorber," Optical Materials Express **6**, 2328-2335 (2016).
27. I. Baylam, F. Canbaz, and A. Sennaroglu, "Dual-Wavelength Temporal Dynamics of a Gain-Switched 2-mu m Tm3+:Lu2O3 Ceramic Laser," IEEE J. Sel. Top. Quantum Electron. **24** (2018).
28. P. Liu, L. Jin, X. Liu, H. T. Huang, J. Zhang, D. Y. Tang, and D. Y. Shen, "A Diode-Pumped Dual-Wavelength Tm, Ho: YAG Ceramic Laser," Ieee Photonics Journal **8** (2016).
29. Y. L. Ju, Z. G. Wang, Y. F. Li, and Y. Z. Wang, "A single-longitudinal-mode dual-wavelength cw Tm,Ho : GdVO4 microchip laser," Chinese Physics Letters **25**, 3250-3252 (2008).
30. C. H. Zhang, B. Q. Yao, G. Li, Q. Wang, Y. L. Ju, and Y. Z. Wang, "2041.3 nm/2054.6 nm Simultaneous Dual-Wavelength Single-Longitudinal-Mode Tm, Ho:YVO4 Microchip Laser," Laser Physics **20**, 1564-1567 (2010).
31. B. B. Wang, C. C. Gao, R. Q. Dou, H. K. Nie, G. H. Sun, W. P. Liu, H. J. Yu, G. J. Wang, Q. L. Zhang, X. C. Lin, J. L. He, W. J. Wang, and B. Y. Zhang, "Dual-wavelength mid-infrared CW and Q-switched laser in diode end-pumped Tm,Ho:GdYTaO4 crystal," Laser Physics Letters **15** (2018).
32. B. M. Walsh, N. P. Barnes, and B. Di Bartolo, "Branching ratios, cross sections, and radiative lifetimes of rare earth ions in solids: Application to Tm3+ and Ho3+ ions in LiYF4," J. Appl. Phys. **83**, 2772-2787 (1998).
33. I. Yorulmaz, and A. Sennaroglu, "Low-Threshold Diode-Pumped 2.3-mu m Tm3+:YLF Lasers," IEEE J. Sel. Top. Quantum Electron. **24** (2018).
34. H. Cankaya, A. T. Gorgulu, A. Kurt, A. Speghini, M. Bettinelli, and A. Sennaroglu, "Comparative Spectroscopic Investigation of Tm3+: Tellurite Glasses for 2-mu m Lasing Applications," Applied Sciences-Basel **8** (2018).
35. U. Demirbas, J. Wang, G. S. Petrich, S. Nabanja, J. R. Birge, L. A. Kolodziejski, F. X. Kartner, and J. G. Fujimoto, "100-nm tunable femtosecond Cr:LiSAF laser mode locked with a broadband saturable Bragg reflector," Appl. Opt. **56**, 3812-3816 (2017).